nature physics

Article

https://doi.org/10.1038/s41567-022-01857-9

Nonlinear multi-frequency phonon lasers with active levitated optomechanics

Received: 12 January 2022

Accepted: 27 October 2022

Published online: 19 January 2023

Check for updates

Tengfang Kuang[1,8], Ran Huang[2,3,8], Wei Xiong[1,4], Yunlan Zuo[2], Xiang Han[1,4], Franco Nori[3,5], Cheng-Wei Qiu[6] ✉, Hui Luo[1] ✉, Hui Jing[2,7] ✉ & Guangzong Xiao[1,4] ✉

Phonon lasers, which exploit coherent amplifications of phonons, are a means to explore nonlinear phononics, image nanomaterial structures and operate phononic devices. Recently, a phonon laser governed by dispersive optomechanical coupling has been demonstrated by levitating a nanosphere in an optical tweezer. Such levitated optomechanical devices, with minimal noise in high vacuum, can allow flexible control of large-mass objects without any internal discrete energy levels. However, it is challenging to achieve phonon lasing with levitated microscale objects because optical scattering losses are much larger than at the nanoscale. Here we report a nonlinear multi-frequency phonon laser with a micro-size sphere, which is governed by dissipative coupling. The active gain provided by a Yb^{3+}-doped system plays a key role. It achieves three orders of magnitude for the amplitude of the fundamental-mode phonon lasing, compared with the passive device. In addition, nonlinear mechanical harmonics can emerge spontaneously above the lasing threshold. Furthermore, we observe coherent correlations of phonons for both the fundamental mode and its harmonics. Our work drives the field of levitated optomechanics into a regime where it becomes feasible to engineer collective motional properties of typical micro-size objects.

Conventional optomechanical systems rely on fixed frames to support mechanical elements, leading to unavoidable energy dissipation and thermal loading[1]. Levitated optomechanical (LOM) systems, that is, controlling motions of levitated objects with optical forces[2], have provided unique advantages[3], such as fundamental minima of damping and noises, the possibility for levitating complex objects, and a high degree of control over both conservative dynamics and coupling to the environment. These advantages are of significance for both fundamental studies of non-equilibrium physics and applications in metrology[4–11]. In recent years, remarkable achievements have been witnessed in LOM systems[12–14], such as the realizations of motional ground-state cooling[15,16], room-temperature strong coupling[17] and ultrahigh-precision torque sensing[18], to name a few. In a recent study[19], a phonon laser or coherent amplification of phonons, the quanta of vibrations, was demonstrated for a levitated nanosphere, based on dispersive LOM coupling, in which the optical resonance frequency is modulated by mechanical motion. This study offers exciting opportunities for exploring the boundary of classical and quantum worlds with

[1]College of Advanced Interdisciplinary Studies, National University of Defense Technology, Changsha, China. [2]Department of Physics and Synergetic Innovation Center for Quantum Effects and Applications, Hunan Normal University, Changsha, China. [3]Quantum Computing Center and Cluster for Pioneering Research, RIKEN, Wako-shi, Japan. [4]Interdisciplinary Center of Quantum Information, National University of Defense Technology, Changsha, China. [5]Physics Department, University of Michigan, Ann Arbor MI, USA. [6]Department of Electrical and Computer Engineering, National University of Singapore, Singapore, Singapore. [7]Synergetic Innovation Academy for Quantum Science and Technology, Zhengzhou University of Light Industry, Zhengzhou, China. [8]These authors contributed equally: Tengfang Kuang, Ran Huang. ✉e-mail: chengwei.qiu@nus.edu.sg; luohui.luo@163.com; jinghui73@foxmail.com; xiaoguangzong@nudt.edu.cn

https://doi.org/10.1038/s41567-022-01857-9

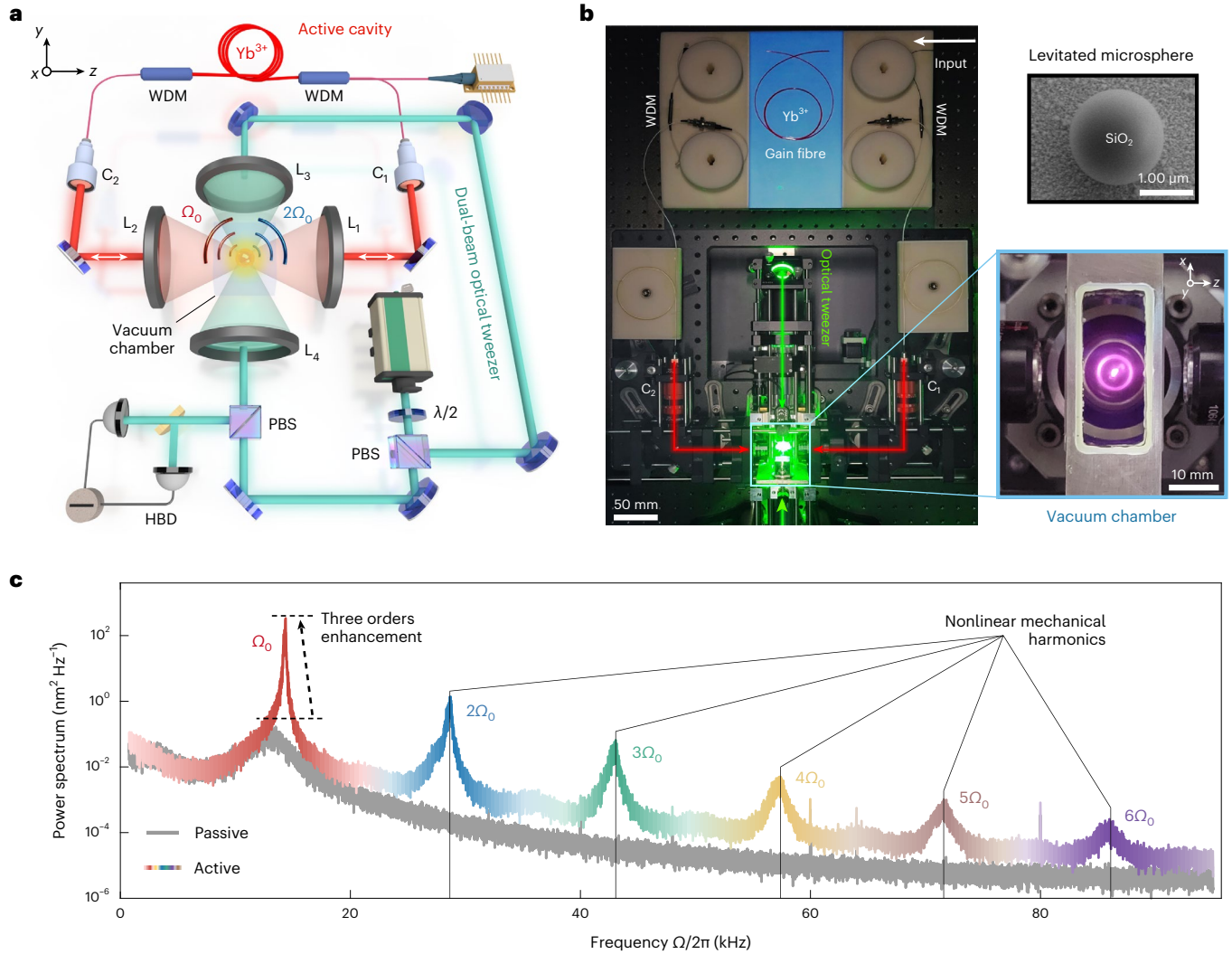

Fig. 1 | Experimental overview. a, Schematic diagram of the active LOM system, including an active optical cavity (red) and a dual-beam optical tweezer (green). WDM, wavelength division multiplexer; C_1 and C_2, collimators; L_1–L_4, lenses; PBS, polarizing beam splitter; $\lambda/2$, half-wave plate; HBD, heterodyne balanced detection. **b**, Photograph of the active LOM set-up with the vacuum chamber and a scanning electron microscope image of the levitated microsphere. **c**, Measured power spectra of phonons in an active cavity (coloured curve) and a passive cavity (grey curve). Here Ω_0 is the frequency of the fundamental mechanical mode.

levitated macroscopic objects[16,20,21], as well as making various levitated sensors[22,23]. Nevertheless, sophisticated feedback controls based on electronic loops[19] are needed to provide both nonlinear cooling and linear heating, and only a single-mode phonon laser was observed, without any evidence of nonlinear mechanical harmonics.

Besides LOM systems, phonon lasers have also been built by using semiconductor superlattices[24], nanomagnets[25], ions[26], and nanomechanical[27] or electromechanical[28] devices. These coherent sound sources, with a shorter wavelength of operation than that of a photon laser of the same frequency[29], are indispensable in steering phonon chips[30], improving the resolution of motional sensors[31] and exploring various effects of phonons[32–34]. However, as far as we know, the ability to achieve multi-frequency phonon lasers with micro-size levitated objects has not been reported. This ability is promising for many important applications, such as multi-frequency motional sensors, exceptional point optomechanics[32,33] and topological sound-wave control[35].

In this Article, we develop a strategy to achieve nonlinear phonon lasers for a levitated object at microscales by utilizing an active LOM system. We show that, in such a system, dissipative LOM coupling[36–39] can be significantly enhanced by introducing an optical gain, thus leading to not only efficient output of fundamental-mode phonon lasing but also spontaneous emergence of mechanical harmonics. The active gain plays a key role in our work as, for passive systems, only thermal phonons exist and no phonon lasing can appear. To steer this system from a chaotic regime into a phonon lasing regime, an optical gain is used to increase the photon lifetime and thus enhance the LOM coupling; as a result, a 3-order enhancement in the power spectrum of the fundamental-mode phonons is achieved, with a 40-fold narrowing in its linewidth. More importantly, above the lasing threshold, we observe nonlinear harmonics with double and triple mechanical frequencies, as clear evidence of gain-enhanced nonlinearity in an active LOM system.

We stress that we achieve phonon lasing with a micro-object, which is three to four orders larger in size or mass than a nanosphere[19]. This ability, which has not been achieved in previous studies[24–28], is an important step towards applications based on coherent motional control of a wide range of typical micro-size objects. Also, our work demonstrates mechanical harmonics accompanying phonon lasing, with evidence of threshold features and high-order correlations. The key role of active gain in enhancing nonlinear LOM effects opens up the

https://doi.org/10.1038/s41567-022-01857-9

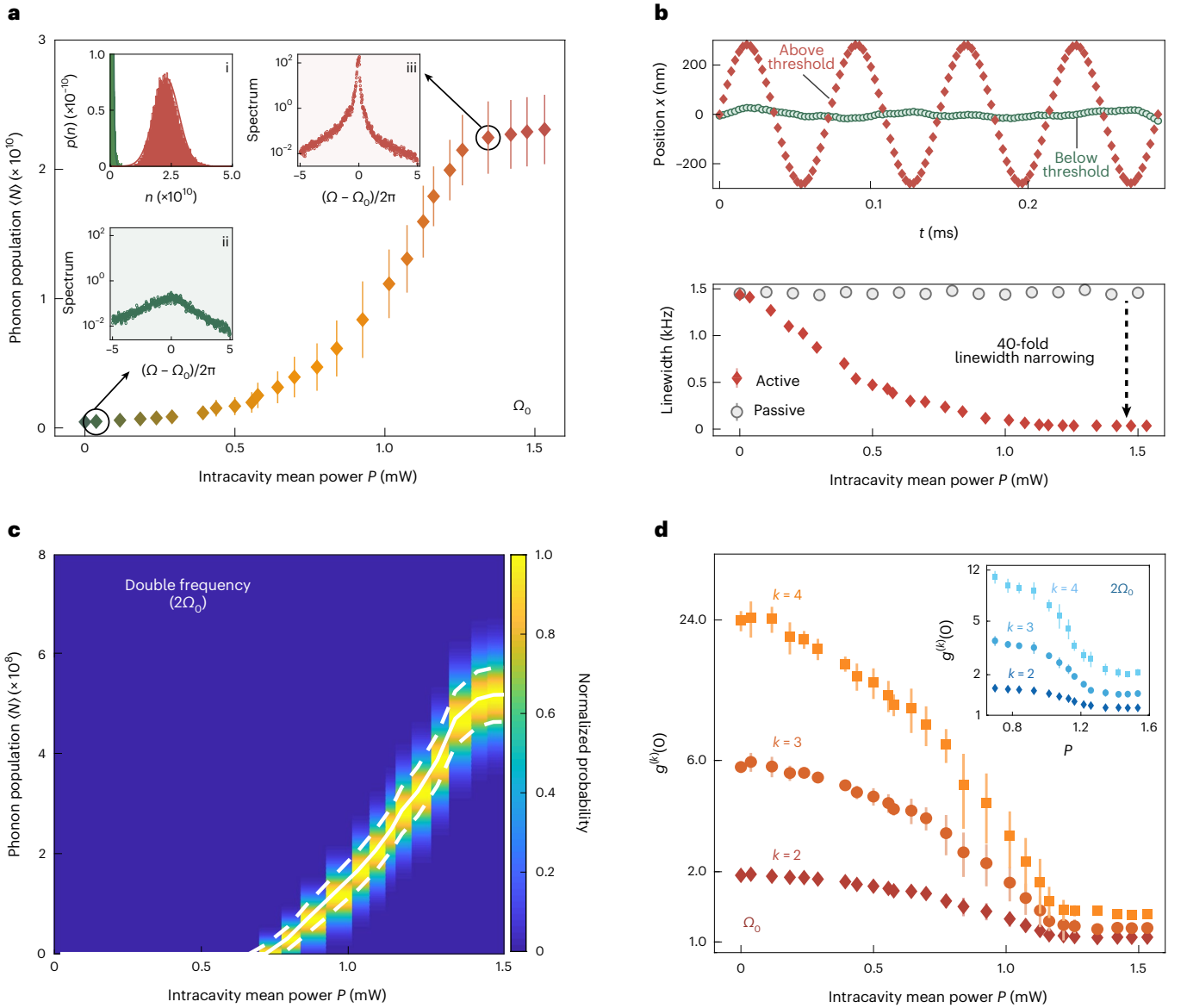

Fig. 2 | Experimental results of phonon lasing with nonlinear harmonics. **a**, Phonon populations $\langle N\rangle$ with fundamental frequency Ω_0 as a function of intracavity mean power P. The measured threshold power is in good agreement with the theoretical prediction. The dots are mean values, and error bars denote ±1 s.d. of each measurement, consisting of 5×10^5 samples. The insets show the phonon probability distributions (i) and the phonon power spectra (ii and iii) below or above the threshold. Here n is the phonon number. **b**, The measured oscillation dynamics (upper) and linewidths (lower) of the fundamental mode by tracing the silicon dioxide (SiO_2) microsphere. **c**, Threshold behaviour of the phonon laser with double frequency $2\Omega_0$ (white solid curve). The solid curve denotes mean value. The white dashed curves represent ±1 s.d. of each measurement, consisting of 5×10^5 samples. The normalized phonon probability distribution is shown in colour. **d**, Measured kth-order phonon autocorrelations at zero-time delay $g^{(k)}(0)$ versus P for Ω_0. Inset: $g^{(k)}(0)$ for $2\Omega_0$. Here the dots represent mean values, and error bars denote ±1 s.d. of each measurement, consisting of 5×10^5 samples.

door to engineer and utilize more nonlinear phononic effects in LOM systems and to achieve exciting goals well beyond the reach of passive systems, for example, parity–time symmetric or gain-enhanced LOM sensing. Finally, our work shows dissipative optomechanical coupling in LOM architectures, and compared with dispersive architectures, dissipative LOM systems are expected to have unique advantages in acoustic metrology[40].

Our experimental platform includes an active optical cavity and a dual-beam optical tweezer for trapping a single microsphere (Fig. 1a,b). The active cavity works for all three translational degrees of freedom, well tunable along both the longitudinal and the vertical directions. Its quality factor is 10^6 but can be enhanced to 10^9 by applying a Yb^{3+}-doped gain fibre. The photon lifetime is thus increased to more than 1 μs, enhancing coherent vibrational amplification of the sphere. Technically, the optical gain is achieved simply by using a Yb^{3+}-doped fibre with a pumping laser at 976 nm, and no other limitation exists. Compared with the cavity-free work[19], there is no need to design and carefully control both nonlinear cooling and linear heating of the mechanical motion with complicated electronic loops or algorithms[19] (see Supplementary Section 1.1 for details).

As shown in Fig. 1c, essentially different features can be observed in the power spectrums of phonons for the cases with or without the gain, that is, only thermal phonons can exist in the passive case, while a three-order-of-magnitude enhancement can be achieved in the active case for the fundamental mode with mechanical frequency $\Omega_0 = 14.4$ kHz. In particular, nonlinear mechanical harmonics with

https://doi.org/10.1038/s41567-022-01857-9

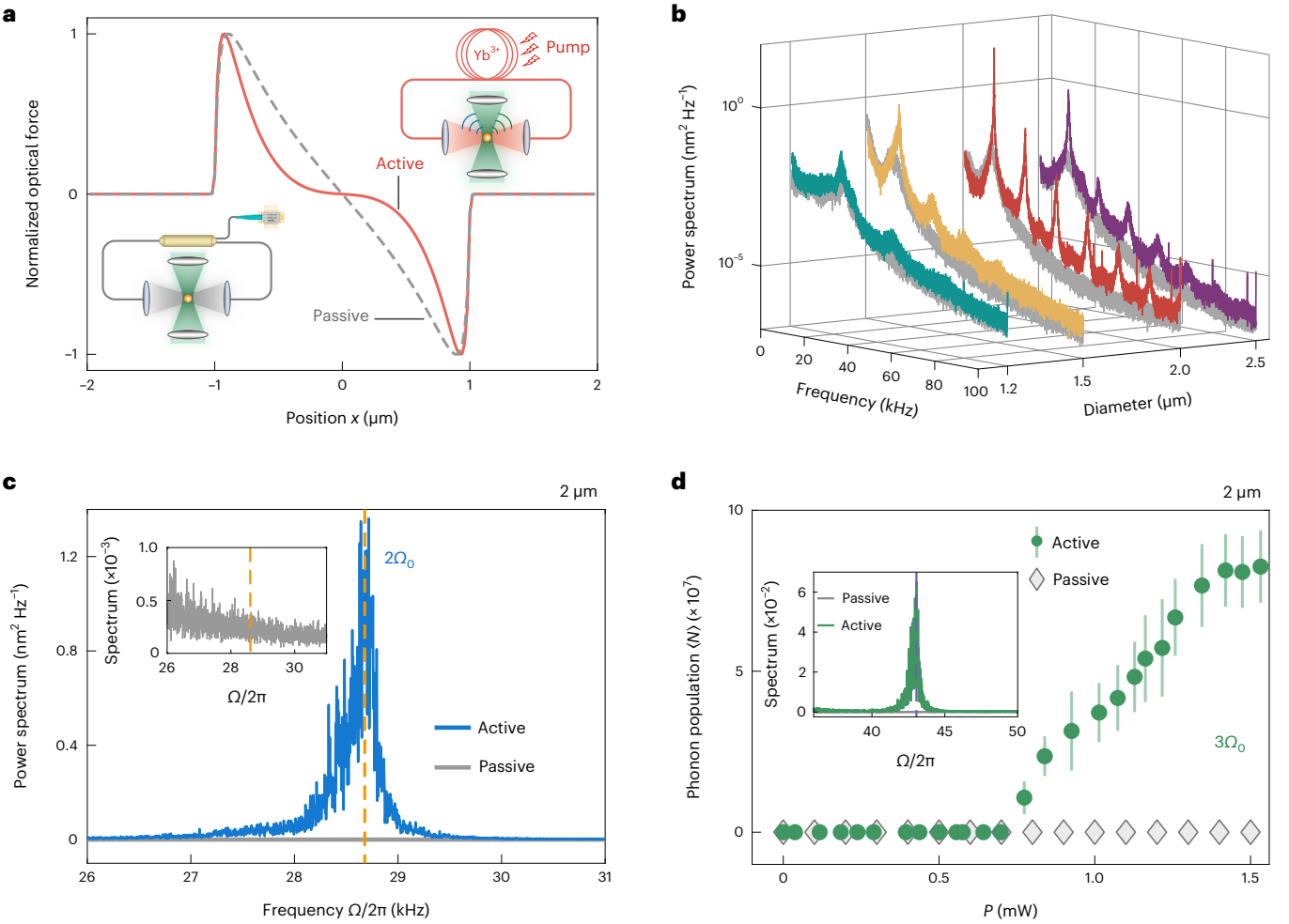

Fig. 3 | Gain-induced phonon lasing with double and triple frequencies. **a**, Normalized optical force distributions for active (red solid curve) and passive (grey dashed curve) cases. The active case shows a strongly nonlinear distribution for the position x between (−1, 1) μm, which is instead linear for the passive case. **b**, Power spectra for spheres of different sizes trapped in active (blue curve) or passive (grey curve) case. **c**, Power spectra around $2\Omega_0$ for such two cases. Inset: 30 times magnified spectrum for better view. **d**, Phonon population with $3\Omega_0$ versus the intracavity mean power P. Phonon laser with $3\Omega_0$ (green dots) or thermal phonons (grey curve) can be clearly observed for different cases, with the corresponding power spectra shown in the inset. Here the dots are mean values, and error bars denote ±1 s.d. of each measurement, consisting of 5×10^5 samples.

frequencies $2\Omega_0$, $3\Omega_0$ and so on emerge spontaneously in the spectrum, enabling the observation of tunable multi-frequency phonon lasers (Supplementary Section 1.4). Besides the role of gain in achieving phonon lasers, we expect that active LOM systems can also serve as an important tool for studying, for example, parity–time symmetric optomechanics[32] or gain-enhanced sound sensing[41].

To confirm the phonon lasing of the fundamental mode and its harmonics, we first measure the steady-state phonon population $\langle N\rangle = M\Omega_0\langle x^2\rangle/\hbar$, where M is the mass of the levitated sphere, Ω_0 is the oscillation frequency of the mode, x is the centre of mass displacement of the sphere and $\hbar$ is the reduced Planck's constant. Explicit signatures of lasing threshold are observed for the fundamental mode, as shown in Fig. 2a, by increasing the intracavity mean power P. The threshold value is $P_{\rm th} = 0.39$ mW, which agrees well with theoretical calculations (Methods). The insets of Fig. 2a showcase a linewidth narrowing, accompanying the transition from thermal to coherent oscillations. Below the threshold, the oscillator features thermal dynamics with mean phonon number 4.63×10^8, and the phonon probability distribution is well described by the Boltzmann distribution. By surpassing the lasing threshold, the phonon number is greatly enhanced towards its saturation value 2.3×10^{10} at $P = 1.3$ mW, also accompanied by a significant narrowing of linewidth. This is closely related to the fact that phonon lasing emerges in the system, resulting in the Gaussian distribution of the generated coherent phonons. By further increasing the power, the phonon population gradually approaches its saturation value.

Figure 2b further presents the experimental results of the dynamical behaviours of the microsphere. We find that significant motional amplifications of the microsphere emerge above the lasing threshold, with a 40-fold improvement in linewidth narrowing, compared with the case without any gain. Clearly, in the passive case, the interaction between the light and the levitated microsphere is rather weak, due to the large optical loss, and the linewidth remains at about 1.5 kHz. In contrast, in the active LOM system, the linewidth can approach as low as 0.03 kHz above the threshold.

Accompanying the giant enhancement of fundamental-mode phonon lasing, we also observe spontaneous emerging of nonlinear mechanical harmonics. We find that similar lasing features for the double-frequency mechanical mode can be achieved as shown in Fig. 2c, which, as far as we know, have not been achieved in LOM systems[19]. It is also different from the multi-mode phonon laser shown in a flat membrane trapped in a Fabry–Pérot cavity[42], in which mode competitions

make it only possible to stimulate a single-phonon mode into the lasing regime.

To further reveal the coherence of the phonon lasers, we study the kth-order phonon autocorrelation functions at zero-time delay $g^{(k)}(0)$ (Supplementary Section 2.2). For the phonon laser in fundamental mode, we find that the kth-order correlations of the phonons satisfy $g_0^{(k)} = k!$ below the threshold $P_{\rm th}$, demonstrating their thermal statistics. As P exceeds $P_{\rm th}$, $g^{(k)}(0)$ decreases and approaches 1, that is, the phonon dynamics changes from the thermal state to the coherent state. Moreover, $g^{(k)}(0)$ approaches 1 for the harmonics with $2\Omega_0$ when operating in the lasing regime, as shown in the inset of Fig. 2d.

We remark that the origin of these nonlinear mechanical harmonics is the anharmonic optical potential produced by the optical-gain-enhanced nonlinearity. Without the gain, for a sphere with larger size than that used in ref. 19, stronger scattering losses lead to a smaller cavity quality factor and thus weaker light–motion coupling. Therefore, we find that the intracavity power P is independent of the x position of the oscillator (Supplementary Section 2.1), while the optical force $F_{\rm opt}$, relying on both P and x, responds linearly to the position x (Fig. 3a). By measuring the phonon dynamics for spheres with different sizes (Fig. 3b), we also find that the linewidth of the fundamental mode is invariant for spheres smaller than 1.2 μm; the phonon lasing only emerges for spheres with larger sizes and becomes stronger when the size is increased to 2 μm. For the active case, the intracavity power can be modulated by the mechanical position due to strong light–motion coupling, and thus we find a strongly nonlinear optical force, as shown in Fig. 3a. As a result, the double-frequency component emerges in the phonon power spectrum (Fig. 3c), with also a giant enhancement compared with the passive case with the same intracavity power $P = 1.3$ mW. Similar lasing features are also observed for the harmonics with the triple-frequency $3\Omega_0$ as shown in Fig. 3d, which is otherwise impossible in the absence of an optical gain.

We note that our results are essentially different from those in a very recent experiment on mechanical parametric amplification[43] that originates from the nonparabolicity of the optical potential and typically dominates in the micrometre region for motional displacement (see also ref. 44). In contrast, in our work, the maximum displacement of the oscillator is ~300 nm, which is small enough and thus far away from the region of observing parametric amplification. In fact, in our work, the nonlinear optical force coming from dissipative LOM coupling exists even for smaller displacements (Supplementary Section 1.2). Moreover, in the parametric amplification system, the nonparabolicity of the optical potential can lead to not only frequency multiplication but also frequency shifts. When the oscillator experiences larger displacements, the absolute value of the optical force is a convex function, the slope of which (and thus the natural frequency of the oscillator) decreases, while, in our work, the natural frequency increases above the lasing threshold. In addition, the origin of the nonlinearity of our work is fundamentally different from that in ref. 19 (see Supplementary Section 1.5 for details). In our future work, by further combining with other existing techniques used in previous studies[19,43], it is possible to probe different nonlinear mechanisms, allowing studies of more nonlinear LOM effects and additional flexible control of LOM devices.

In summary, we have experimentally demonstrated a nonlinear phonon laser in an active LOM system. By introducing optical gain, we have realized a phonon laser on the fundamental mode with a three-order-of-magnitude enhancement in the power spectrum and a 40-fold improvement in linewidth narrowing, without the need of any complicated external feedback control techniques. We also present unequivocal evidence of lasing threshold behaviour and the phase transition from thermal to coherent phonons by measuring the phonon autocorrelations. More interestingly, we observe nonlinear phonon lasers with multiple frequencies, resulting from the optical-gain-enhanced nonlinearity. This observation of such nonlinear mechanical harmonics in LOM systems does not rely on the specific material or the shape of the oscillator[45,46]. We measured also correlations $g^{(k)}(0)$ of harmonic phonon lasing. These results push phonon lasers into the nonlinear regime and make many exciting applications more accessible, such as optomechanical combs[47], high-precision metrology and non-classical state engineering. Our work opens up perspectives for achieving levitated phonon devices with active LOM systems and enables a wide range of applications, such as quantum phononics, multi-frequency mechanical sensors and high-precision acoustic frequency combs.

We stress that the purpose of our work is not to outperform dispersive phonon lasers; instead, it enriches the present toolbox of phonon lasing by confirming that, even for a micro-object containing as many as $\sim 10^{11}$ atoms, that is, four orders of magnitude higher than that used in ref. 19, it is still possible to achieve collective mechanical amplifications and observe the accompanying nonlinear effects. In fact, our work can be combined with existing techniques from previous studies, for future studies of more exciting projects, for example, switch phonon lasing from dissipative-coupling-governed regime to dispersive-coupling-governed regime, transient LOM effects with comparable couplings and the role of gain in operating nonlinear phonon lasers for sound-sensing applications.

Note added in proof: When submitting our revised manuscript, an experiment appeared[40], and in that work, different features of dispersive and dissipative couplings in sound sensing are compared, by using a different system, that is, a suspended fibre coupled with an optical resonator.

Online content

Any methods, additional references, Nature Portfolio reporting summaries, source data, extended data, supplementary information, acknowledgements, peer review information; details of author contributions and competing interests; and statements of data and code availability are available at https://doi.org/10.1038/s41567-022-01857-9.

References

1. Millen, J., Monteiro, T. S., Pettit, R. & Vamivakas, A. N. Optomechanics with levitated particles. *Rep. Prog. Phys.* **83**, 026401 (2020).
2. Ashkin, A. Acceleration and trapping of particles by radiation pressure. *Phys. Rev. Lett.* **24**, 156–159 (1970).
3. Gonzalez-Ballestero, C., Aspelmeyer, M., Novotny, L., Quidant, R. & Romero-Isart, O. Levitodynamics: levitation and control of microscopic objects in vacuum. *Science* **374**, eabg3027 (2021).
4. Gieseler, J., Novotny, L. & Quidant, R. Thermal nonlinearities in a nanomechanical oscillator. *Nat. Phys.* **9**, 806–810 (2013).
5. Ranjit, G., Cunningham, M., Casey, K. & Geraci, A. A. Zeptonewton force sensing with nanospheres in an optical lattice. *Phys. Rev. A* **93**, 053801 (2016).
6. Moore, D. C., Rider, A. D. & Gratta, G. Search for millicharged particles using optically levitated microspheres. *Phys. Rev. Lett.* **113**, 251801 (2014).
7. Frimmer, M. et al. Controlling the net charge on a nanoparticle optically levitated in vacuum. *Phys. Rev. A* **95**, 061801 (2017).
8. Jackson Kimball, D. F., Sushkov, A. O. & Budker, D. Precessing ferromagnetic needle magnetometer. *Phys. Rev. Lett.* **116**, 190801 (2016).
9. Monteiro, F. et al. Force and acceleration sensing with optically levitated nanogram masses at microkelvin temperatures. *Phys. Rev. A* **101**, 053835 (2020).
10. Hebestreit, E., Frimmer, M., Reimann, R. & Novotny, L. Sensing static forces with free-falling nanoparticles. *Phys. Rev. Lett.* **121**, 063602 (2018).
11. Rider, A. D. et al. Search for screened interactions associated with dark energy below the 100 μm length scale. *Phys. Rev. Lett.* **117**, 101101 (2016).

12. Chang, D. E. et al. Cavity opto-mechanics using an optically levitated nanosphere. *Proc. Natl Acad. Sci. USA* **107**, 1005–1010 (2010).
13. Barker, P. F. & Shneider, M. N. Cavity cooling of an optically trapped nanoparticle. *Phys. Rev. A* **81**, 023826 (2010).
14. Romero-Isart, O., Juan, M. L., Quidant, R. & Cirac, J. I. Toward quantum superposition of living organisms. *New J. Phys.* **12**, 033015 (2010).
15. Li, T., Kheifets, S. & Raizen, M. G. Millikelvin cooling of an optically trapped microsphere in vacuum. *Nat. Phys.* **7**, 527–530 (2011).
16. Delić, U. et al. Cooling of a levitated nanoparticle to the motional quantum ground state. *Science* **367**, 892–895 (2020).
17. de los Ríos Sommer, A., Meyer, N. & Quidant, R. Strong optomechanical coupling at room temperature by coherent scattering. *Nat. Commun.* **12**, 276 (2021).
18. Hoang, T. M. et al. Torsional optomechanics of a levitated nonspherical nanoparticle. *Phys. Rev. Lett.* **117**, 123604 (2016).
19. Pettit, R. M. et al. An optical tweezer phonon laser. *Nat. Photon.* **13**, 402–405 (2019).
20. Magrini, L. et al. Real-time optimal quantum control of mechanical motion at room temperature. *Nature* **595**, 373–377 (2021).
21. Tebbenjohanns, F., Mattana, M. L., Rossi, M., Frimmer, M. & Novotny, L. Quantum control of a nanoparticle optically levitated in cryogenic free space. *Nature* **595**, 378–382 (2021).
22. Hoang, T., Ahn, J., Bang, J. & Li, T. Electron spin control of optically levitated nanodiamonds in vacuum. *Nat. Commun.* **7**, 12250 (2016).
23. Gieseler, J. et al. Single-spin magnetomechanics with levitated micromagnets. *Phys. Rev. Lett.* **124**, 163604 (2020).
24. Trigo, M., Bruchhausen, A., Fainstein, A., Jusserand, B. & Thierry-Mieg, V. Confinement of acoustical vibrations in a semiconductor planar phonon cavity. *Phys. Rev. Lett.* **89**, 227402 (2002).
25. Chudnovsky, E. M. & Garanin, D. A. Phonon superradiance and phonon laser effect in nanomagnets. *Phys. Rev. Lett.* **93**, 257205 (2004).
26. Vahala, K. J. et al. A phonon laser. *Nat. Phys.* **5**, 682–686 (2009).
27. Bargatin, I. & Roukes, M. L. Nanomechanical analog of a laser: amplification of mechanical oscillations by stimulated Zeeman transitions. *Phys. Rev. Lett.* **91**, 138302 (2003).
28. Mahboob, I., Nishiguchi, K., Fujiwara, A. & Yamaguchi, H. Phonon lasing in an electromechanical resonator. *Phys. Rev. Lett.* **110**, 127202 (2013).
29. Li, N. et al. Colloquium: Phononics: manipulating heat flow with electronic analogs and beyond. *Rev. Mod. Phys.* **84**, 1045–1066 (2012).
30. Hackett, L. et al. Towards single-chip radiofrequency signal processing via acoustoelectric electron–phonon interactions. *Nat. Commun.* **12**, 2769 (2021).
31. Cui, K. et al. Phonon lasing in a hetero optomechanical crystal cavity. *Photon. Res.* **9**, 937–943 (2021).
32. Jing, H. et al. PT-symmetric phonon laser. *Phys. Rev. Lett.* **113**, 053604 (2014).
33. Zhang, J. et al. A phonon laser operating at an exceptional point. *Nat. Photon.* **12**, 479–484 (2018).
34. Jiang, Y., Maayani, S., Carmon, T., Nori, F. & Jing, H. Nonreciprocal phonon laser. *Phys. Rev. Appl.* **10**, 064037 (2018).
35. Serra-Garcia, M. et al. Observation of a phononic quadrupole topological insulator. *Nature* **555**, 342 (2018).
36. Elste, F., Girvin, S. M. & Clerk, A. A. Quantum noise interference and backaction cooling in cavity nanomechanics. *Phys. Rev. Lett.* **102**, 207209 (2009).
37. Kalantarifard, F. et al. Intracavity optical trapping of microscopic particles in a ring-cavity fiber laser. *Nat. Commun.* **10**, 2683 (2019).
38. Kuang, T. et al. Dual-beam intracavity optical trap with all-optical independent axial and radial self-feedback schemes. *Opt. Express* **29**, 29936 (2021).
39. Leefmans, C. et al. Topological dissipation in a time-multiplexed photonic resonator network. *Nat. Phys.* **18**, 442 (2022).
40. Meng, J.-W. et al. Dissipative acousto-optic interactions in optical microcavities. *Phys. Rev. Lett.* **129**, 073901 (2022).
41. Peano, V., Schwefel, H. G. L., Marquardt, Ch. & Marquardt, F. Intracavity squeezing can enhance quantum-limited optomechanical position detection through deamplification. *Phys. Rev. Lett.* **115**, 243603 (2015).
42. Kemiktarak, U., Durand, M., Metcalfe, M. & Lawall, J. Mode competition and anomalous cooling in a multimode phonon laser. *Phys. Rev. Lett.* **113**, 030802 (2014).
43. Zheng, Y. et al. Robust optical-levitation-based metrology of nanoparticle's position and mass. *Phys. Rev. Lett.* **124**, 223603 (2020).
44. Li, T. *Fundamental Tests of Physics with Optically Trapped Microspheres* Ch. 2 (Springer Science & Business Media, 2012).
45. Grudinin, I. S., Lee, H., Painter, O. & Vahala, K. J. Phonon laser action in a tunable two-level system. *Phys. Rev. Lett.* **104**, 083901 (2010).
46. Asano, M. et al. Observation of optomechanical coupling in a microbottle resonator. *Laser Photon. Rev.* **10**, 603–611 (2016).
47. Ip, M. et al. Phonon lasing from optical frequency comb illumination of trapped ions. *Phys. Rev. Lett.* **121**, 043201 (2018).

Methods

Experimental details

A dual-beam optical tweezer and an active optical cavity are used in our experimental apparatus. These two set-ups are vertical to each other around the trapping region as shown in Extended Data Fig. 1. A silica sphere is trapped by the dual-beam optical tweezer inside a tiny chamber (Extended Data Fig. 1a, inset). Extended Data Fig. 1b shows a diagram of the experimental set-up. The origin of the cylindrical coordinate system is located at the lens's focal point of the dual-beam optical tweezer. We install the free-space laser path of the active cavity to a three-dimensional translation stage. The relative position of the active cavity to the trapped sphere can be tuned. A balanced photodetector is installed to monitor the centre of mass displacement of the trapped sphere. There is no need for any external hardware or software to implement feedback control.

The trapping power of the dual-beam optical tweezer (>100 mW) is much stronger than that of the active cavity (~1 mW), which can produce robust restoring force to trap the sphere. The wavelength of the low-noise laser (Laser Quantum, Axiom 532) is far away from the absorption spectrum of Yb^{3+}, thus minimizing its influence on the active cavity. We equally split the trapping laser into s- and p-polarized parts by using a halfwave plate and a polarizing beam splitter (PBS_1). Then, the s- and p-polarized light can be focused on the sphere through two high-numerical-aperture (NA) objectives L_3 and L_4 (Mitutoyo, M Plan Apo 100x, NA = 0.7). The portion of the s-polarized light scattered from the sphere is channelled by the PBS_2 to a beam splitter whose outputs are then sent to a balanced photodetector (BPD). As the sphere alters the spatial distribution of the scattering light, the differential mode signal from the BPD reveals the sphere's position[48].

The active cavity comprises a continuous-wave ring-cavity fibre laser emitting along with the clockwise and anticlockwise directions. We use a single-mode Yb^{3+}-doped fibre (nLIGHT, Yb1200-6/125, core diameter of 6 μm, cladding diameter of 125 μm) as a gain medium, pumped by a single-mode diode laser at 976 nm through wavelength division multiplexer (WDM_1). The residual part of the pump laser is coupled out of the ring cavity through WDM_2. The emitted lasers, centred at 1,030 nm, are expanded to free space by collimators C_1 and C_2 and then focused onto the trapped sphere using two collimating objective lenses L_1 and L_2 (NA = 0.25). The lenses are specially coated to enhance transmissivity and reduce their influence on the cavity loss. Collimators C_1 and C_2 are then used to couple the transmitted light through the trapping region back into the fibre loop. We tune the intracavity laser power (0–1.2 mW) by adjusting the power of the pump laser. Photodetectors PD_1 and PD_2 are installed to monitor the clockwise and anticlockwise laser powers.

We have confirmed that in our experiment, if there is no active medium, no phonon lasing can appear for micro-size levitated spheres, due to strong optical scattering losses. Thus, in our system, the active feedback plays a key role in compensating losses and achieving the nonlinear phonon laser. As already confirmed in our experiment, our active cavity indeed works for all three translational degrees of freedom, with well-tunable feedbacks along the longitudinal and vertical directions (by regulating the foci distance of the trapping beam). The optical gain is achieved by using a Yb^{3+}-doped fibre with a pumping laser at 976 nm. As far as we know, no other limitation exists in our experiment. We expect that our active LOM system can also be an important tool for studying, for example, parity–time symmetric optomechanics and gain-enhanced metrology.

Cavity alignment

We mount the pumping laser to one collimator (Thorlabs, ZC618FC-B) and a power meter to another. The alignment is evaluated by the coupling coefficient from one collimator to another. Through adjusting the lenses and mirrors, the loss of the free-space optical path can be regulated to its lowest value (usually lower than 0.31 dB).

Microsphere trapping

The sphere was loaded into the trapping region by using an ultrasonic nebulizer, composed of an ultrasonic sheet metal with a great number of 5 μm holes distributed. It was trapped at atmospheric pressure. In most cases, a microsphere can be trapped within 30 s. Then, we reduced the pressure to the desired experimental level.

Phonon population distribution

The phonon population is obtained according to the relationship $\langle N\rangle = M\Omega_0\langle x^2\rangle/\hbar$, where M is the mass of the levitated sphere, Ω_0 is the oscillation frequency of the mechanical mode, $\langle x^2\rangle$ is the mean squared displacement of the sphere's centre of mass and $\hbar$ is the reduced Planck's constant. Given a series of trajectories x_i with $i = 1, \ldots, L$, the distribution $\rho(n)$ is constructed as follows. First, starting from $i = 1$, extract a finite dataset from x_i with length k. Loop all datasets to calculate the phonon population as $N_j = \frac{M\Omega_0}{\hbar}\frac{1}{k}\sum_{i=j}^{k}(x_i - \bar{x})^2$, where $j = 1,\ldots,i$, and $\bar{x} = \langle x\rangle$. Second, determine the common maximum and minimum value of the phonon population variable, denoted by $N_{\max}$ and $N_{\min}$, and discretize the interval $[N_{\max}, N_{\min}]$ into P bins as $N_\alpha = N_{\min} + \frac{\alpha}{P}(N_{\max} - N_{\min})$, $\alpha = 0, 1, \ldots, P-1$, where P is the total number of bins and α is a particular bin's number. Then, use the ith time series to calculate the frequency of data points falling in each subinterval, obtaining the distribution for the experiments $\rho(n)$.

Theoretical model

The dissipative optomechanical system, with the first-order dissipative optomechanical coupling $\kappa(x) \approx \kappa + g_\kappa x$, can be described via the Hamiltonian[49]

$$\hat{H} = \hbar\Delta\hat{a}^\dagger\hat{a} + \frac{1}{2}\hbar\omega_{\mathrm{M}}\left(\hat{Q}^2 + \hat{P}^2\right) + i\hbar\sqrt{2\kappa}\left(1 + \frac{\sqrt{2}g}{2\kappa}\hat{Q}\right)\left[\hat{a}^\dagger\left(\varepsilon_{\mathrm{l}} + \hat{c}_{\mathrm{l}}\right) - \hat{a}\left(\varepsilon_{\mathrm{l}} + \hat{c}_{\mathrm{l}}^\dagger\right)\right], \tag{1}$$

where $\hat{a}$ ($\hat{a}^\dagger$) are the annihilation (creation) operators of the cavity field satisfying the commutation relation $[\hat{a}, \hat{a}^\dagger] = 1$; $\Delta = \omega_{\mathrm{C}} - \omega_{\mathrm{l}}$ is the cavity detuning with respect to the frequency of the input laser; $\hat{Q} = \hat{x}/(\sqrt{2}x_{\mathrm{zpt}})$ and $\hat{P} = \hat{p}/(\sqrt{2}p_{\mathrm{zpt}})$ are the dimensionless position and momentum operators of the oscillator with zero-point motion $x_{\mathrm{zpt}} = \sqrt{\hbar/2m\omega_{\mathrm{M}}}$ and zero-point momentum $p_{\mathrm{zpt}} = \sqrt{\hbar m\omega_{\mathrm{M}}/2}$, respectively, satisfying the commutation relation $[\hat{Q}, \hat{P}] = i$; ω_{M} and m are the frequency and mass of the mechanical oscillator; $\varepsilon_{\mathrm{l}} = \sqrt{P_{\mathrm{in}}/(\hbar\omega_{\mathrm{l}})}$ is the amplitude of the input laser related to the input power P_{in} and the input vacuum noise $\hat{c}_{\mathrm{l}}$; and the dissipative coupling constant is $g = g_\kappa x_{\mathrm{zpt}}$.

Using the Heisenberg equations of motion $\dot{\hat{\mathcal{O}}} = -\mathrm{i}[\hat{\mathcal{O}}, \hat{H}]/\hbar$ and adding the corresponding damping and noise terms, the quantum Langevin equations of the system operators are given by

$$\begin{aligned}
\dot{\hat{Q}} &= \omega_{\mathrm{M}}\hat{P},\\
\dot{\hat{P}} &= -\omega_{\mathrm{M}}\hat{Q} - i\tfrac{g}{\sqrt{\kappa}}[\hat{a}^\dagger(\varepsilon_{\mathrm{l}} + \hat{c}_{\mathrm{l}}) - \hat{a}(\varepsilon_{\mathrm{l}} + \hat{c}_{\mathrm{l}}^\dagger) - \sqrt{2\kappa}\hat{a}^\dagger\hat{a}] - \gamma_{\mathrm{M}}\hat{P} + \hat{\xi},\\
\dot{\hat{a}} &= -[i\Delta + (\kappa + \sqrt{2}g\hat{Q} - G)]\hat{a} + \sqrt{2\kappa}\left(1 + \tfrac{\sqrt{2}g}{2\kappa}\hat{Q}\right)(\varepsilon_{\mathrm{l}} + \hat{c}_{\mathrm{l}}),
\end{aligned} \tag{2}$$

where the input vacuum noise operator $\hat{c}_{\mathrm{l}}$ has zero mean value and delta correlation $\langle\hat{c}_{\mathrm{l}}(t)\hat{c}_{\mathrm{l}}^\dagger(t')\rangle = \delta(t - t')$, where δ indicates the Dirac delta function; G is the optical gain of the active cavity; and ξ is the thermal noise with zero mean value and following correlation function $\langle\xi(t)\xi^\dagger(t')\rangle = \frac{1}{2\pi}\frac{\Gamma_{\mathrm{M}}}{\omega_{\mathrm{M}}}\int\omega\mathrm{e}^{-\mathrm{i}\omega(t-t')}\left[1 + \coth\left(\frac{\hbar\omega}{2k_{\mathrm{B}}T}\right)\right]\mathrm{d}\omega$, where k_{B} is the Boltzmann constant, t is time and T is temperature. By setting the time derivatives in above equations to 0, we find the steady state of the dynamical variables:

$$\bar{Q} = i\frac{g\varepsilon_{\mathrm{l}}}{\omega_{\mathrm{M}}\sqrt{\kappa}}(\bar{a} - \bar{a}^*),\ \bar{a} = \frac{\left(\sqrt{2\kappa} + \frac{g}{\sqrt{\kappa}}\bar{Q}\right)\varepsilon_{\mathrm{l}}}{i\Delta + \kappa + \sqrt{2}g\bar{Q} - G}. \tag{3}$$

Now we consider $\hat{c}_l(\hat{c}_l^\dagger)$ as the annihilation (creation) operator of the input field satisfying the commutation relation $[\hat{c}_l, \hat{c}_l^\dagger] = 1$. The Hamiltonian can be rewritten as

$$\begin{aligned}
\hat{H} &= \hat{H}_0 + \hat{H}_{\rm int} + \hat{H}_{\rm dr},\\
\hat{H}_0 &= \hbar(\Delta - i\kappa + iG)\hat{a}^\dagger\hat{a} + \hbar\omega_{\rm M}\hat{b}^\dagger\hat{b},\\
\hat{H}_{\rm int} &= -i\hbar g\left(\hat{b}^\dagger + \hat{b}\right)\hat{a}^\dagger\hat{a} + i\hbar\sqrt{2\kappa}\left(\hat{a}^\dagger\hat{c}_l - \hat{a}\hat{c}_l^\dagger\right),\\
\hat{H}_{\rm dr} &= i\hbar\sqrt{2\kappa}\varepsilon_l\left(\hat{a}^\dagger - \hat{a}\right),
\end{aligned} \tag{4}$$

where $\hat{b}(\hat{b}^\dagger)$ are the annihilation (creation) operator of the mechanical mode. We introduce the supermode operators $\hat{a}_+ = (\hat{a} + i\hat{c}_l)/\sqrt{2}$ and $\hat{a}_- = (\hat{a} - i\hat{c}_l)/\sqrt{2}$, which satisfy the commutation relations $\left[\hat{a}_+, \hat{a}_+^\dagger\right] = \left[\hat{a}_-, \hat{a}_-^\dagger\right] = 1$ and $[\hat{a}_+, \hat{a}_-] = \left[\hat{a}_+, \hat{a}_-^\dagger\right] = 0$. Under the rotating-wave approximation, $2\sqrt{2\kappa} + \omega_{\rm M}$ and $\omega_{\rm M}$ are much larger than $\left|2\sqrt{2\kappa} - \omega_{\rm M}\right|$, and the equations of motion of the system are given by

$$\begin{aligned}
\dot{\hat{a}}_+ &= -(i\omega_+ + \gamma)\hat{a}_+ - \left(\tfrac{g}{2}\hat{b} + \gamma + i\tfrac{\Delta}{2}\right)\hat{a}_- + \sqrt{\kappa}\varepsilon_l,\\
\dot{\hat{a}}_- &= -(i\omega_- + \gamma)\hat{a}_- - \left(\tfrac{g}{2}\hat{b}^\dagger + \gamma + i\tfrac{\Delta}{2}\right)\hat{a}_+ + \sqrt{\kappa}\varepsilon_l,\\
\dot{\hat{p}} &= -2\left(\gamma + i\sqrt{2\kappa}\right)\hat{p} + \left(\tfrac{g}{2}\hat{b} + \gamma + i\tfrac{\Delta}{2}\right)\delta\hat{n} + \sqrt{\kappa}\varepsilon_l(\hat{a}_-^\dagger + \hat{a}_+),\\
\dot{\hat{b}} &= -(i\omega_{\rm M} + \gamma_{\rm M})\hat{b} - \tfrac{g}{2}\hat{p},
\end{aligned} \tag{5}$$

where $\hat{p} = \hat{a}_-^\dagger\hat{a}_+$ and $\delta\hat{n} = \hat{a}_+^\dagger\hat{a}_+ - \hat{a}_-^\dagger\hat{a}_-$ are the ladder operator and the population inversion operator, respectively; $\omega_\pm = \frac{\Delta}{2} \pm \sqrt{2\kappa}$; $\gamma = \frac{\kappa - G}{2}$; and $\gamma_{\rm M}$ denotes the damping of the oscillator. Since $\gamma \gg \gamma_{\rm M}$, we can adiabatically eliminate the degrees of freedom of the optical modes by setting the time derivatives of the optical components to 0. Then, we obtain the steady-state values:

$$\begin{aligned}
a_+ &= \frac{\sqrt{\kappa}\varepsilon_l\left(-gb - i2\sqrt{2\kappa}\right)}{\beta - i\zeta},\\
a_- &= \frac{\sqrt{\kappa}\varepsilon_l\left(-gb^* + i2\sqrt{2\kappa}\right)}{\beta - i\zeta},\\
p &= \frac{2\sqrt{\kappa}\varepsilon_l\left(a_-^\dagger + a_+\right) + (gb + 2\gamma + i\Delta)\Delta n}{4\gamma + i2\left(2\sqrt{2\kappa} - \omega_{\rm M}\right)},
\end{aligned} \tag{6}$$

with $\beta = \beta_0 - (\kappa - G)\frac{gQ}{\sqrt{2}}$, $\beta_0 = 4\kappa - \frac{g^2}{2}n_b$, $\zeta = \frac{\Delta gQ}{\sqrt{2}}$, and the mean phonon number $n_b = b^\dagger b$.

Then, the dynamics of the mechanical oscillator can be described by $\dot{b} = (G_{\rm M} - \gamma_{\rm M} - i\omega_{\rm M} - i\omega_{\rm M}')b - D$, where the parameters $\omega_{\rm M}'$ and D can be obtained by comparing this motion equation with equation (7). The effective mechanical gain is given by

$$G_{\rm M} = \frac{(G - \kappa)g^2/4}{(G - \kappa)^2 + \left(2\sqrt{2\kappa} - \omega_{\rm M}\right)^2}\left(\delta n - \frac{4\kappa\beta\varepsilon_l^2}{\beta^2 + \zeta^2}\right). \tag{7}$$

By setting $G_{\rm M} = \gamma_{\rm M}$ and assuming that the phonon laser satisfies the condition of complete inversion $\delta n \approx n_+$, we obtain the threshold of the phonon laser with $P_{\rm th} = \hbar\omega_+(G - \kappa)n_+$, that is

$$\begin{aligned}
P_{\rm th} &= P_{\rm th,0} + P_{\rm th,1},\\
P_{\rm th,0} &= 2\tfrac{\hbar\gamma_{\rm M}}{g^2}\left(\Delta + 2\sqrt{2\kappa}\right)\left[\left(2\sqrt{2\kappa} - \omega_{\rm M}\right)^2 + (G - \kappa)^2\right]\\
&+ \frac{2\hbar\kappa\beta\varepsilon_l^2}{\beta^2 + \zeta^2}\left(\Delta + 2\sqrt{2\kappa}\right)(G - \kappa),\\
P_{\rm th,1} &= \frac{2\hbar\kappa\beta\varepsilon_l^2\left(\Delta + 2\sqrt{2\kappa}\right)(G - \kappa)}{\beta^2 + \zeta^2}.
\end{aligned} \tag{8}$$

Phonon correlations

The normalized equal-time kth-order phonon correlation is given by[50]

$$\begin{aligned}
g^{(k)}(0) &= \frac{\left\langle\hat{b}^{\dagger k}\hat{b}^k\right\rangle}{\left\langle\hat{b}^\dagger\hat{b}\right\rangle^k} = \langle\hat{N}\rangle^{-k}\sum_{N=k}^{\infty}N(N-1)\cdots(N-k+1)P(N)\\
&= \sum_{N=k}^{\infty}\frac{N!}{(N-k)!}\frac{P(N)}{\langle\hat{N}\rangle^k}
\end{aligned} \tag{9}$$

In particular, the second-order phonon correlation function is

$$g^{(2)}(0) = \frac{\left\langle\hat{b}^{\dagger 2}\hat{b}^2\right\rangle}{\left\langle\hat{b}^\dagger\hat{b}\right\rangle^2} = \frac{\langle\hat{N}(\hat{N}-1)\rangle}{\langle\hat{N}\rangle^2} = \frac{\langle\hat{N}\rangle^2 - \langle\hat{N}\rangle}{\langle\hat{N}\rangle^2} \tag{10}$$

The third-order and fourth-order phonon correlation functions are $g^{(3)}(0) = \left(\langle\hat{N}^3\rangle - 3\langle\hat{N}^2\rangle + 2\langle\hat{N}\rangle\right)/\langle\hat{N}\rangle^3$ and $g^{(4)}(0) = \left(\langle N^4\rangle - 6\langle\hat{N}^3\rangle + 11\langle\hat{N}^2\rangle - 6\langle\hat{N}\rangle\right)/\langle\hat{N}\rangle^4$, respectively.

Data availability

Source data are available for this paper. All other data that support the plots within this paper and other findings of this study are available from the corresponding authors upon reasonable request.

Code availability

The computer codes that were used to generate the data that support the findings of this study are available from the corresponding authors upon reasonable request.

References

48. Li, T., Kheifets, S., Medellin, D. & Raizen, M. G. Measurement of the instantaneous velocity of a Brownian particle. *Science* **328**, 1673–1675 (2010).
49. Huang, S. & Chen, A. Improving the cooling of a mechanical oscillator in a dissipative optomechanical system with an optical parametric amplifier. *Phys. Rev. A* **98**, 063818 (2018).
50. Glauber, R. J. *The Quantum Theory of Optical Coherence* (Wiley-VCH, 2007).

Acknowledgements

We gratefully acknowledge the valuable assistance from B. Luo at the Beijing University of Posts and Telecommunications (BUPT), Y. Jiao and X. Xu at Hunan Normal University (HNU) and Z. Liu, W. Zeng and X. Chen at the National University of Defense Technology (NUDT). H.J. and F.N. thank Ş. K. Özdemir for discussions. X.G. is supported by the National Natural Science Foundation of China (NSFC, grant no. 61975237). H.J. is supported by the NSFC (grant nos. 11935006 and 11774086) and the Science and Technology Innovation Program of Hunan Province (grant no. 2020RC4047). X.H. is supported by the Independent Scientific Research Project of NUDT (grant no. ZZKY-YX-07-02). W.X. is supported by the Scientific Research Project of NUDT (grant no. ZK20-14). X. Chen is supported by the NSFC (grant no. 11904405). R.H. acknowledges support from the Japan Society for the Promotion of Science (JSPS) Postdoctoral Fellowships for Research in Japan (no. P22018). F.N. acknowledges partial support from NTT Research, JSPS (JP20H00134), AOARD (FA2386-20-1-4069) and FQXi (FQXi-IAF19-06).

Author contributions

X.G. and H.J. conceived the idea. T.K. and X.G. designed the experiments. T.K., W.X. and X.H. performed the experiments and analysed the experimental data with the help of X.G. R.H. and T.K. performed the theoretical analysis and numerical simulations, guided by H.J. R.H., T.K. and Y.Z. wrote the manuscript with contributions from X.G., H.J., F.N. and C.-W.Q. X.G., H.J. and H.L. supported the project.

Competing interests
The authors declare no competing interests.

Additional information
Extended data is available for this paper at https://doi.org/10.1038/s41567-022-01857-9.

Supplementary information The online version contains supplementary material available at https://doi.org/10.1038/s41567-022-01857-9.

Correspondence and requests for materials should be addressed to Cheng-Wei Qiu, Hui Luo, Hui Jing or Guangzong Xiao.

Peer review information *Nature Physics* thanks the anonymous reviewers for their contribution to the peer review of this work.

https://doi.org/10.1038/s41567-022-01857-9

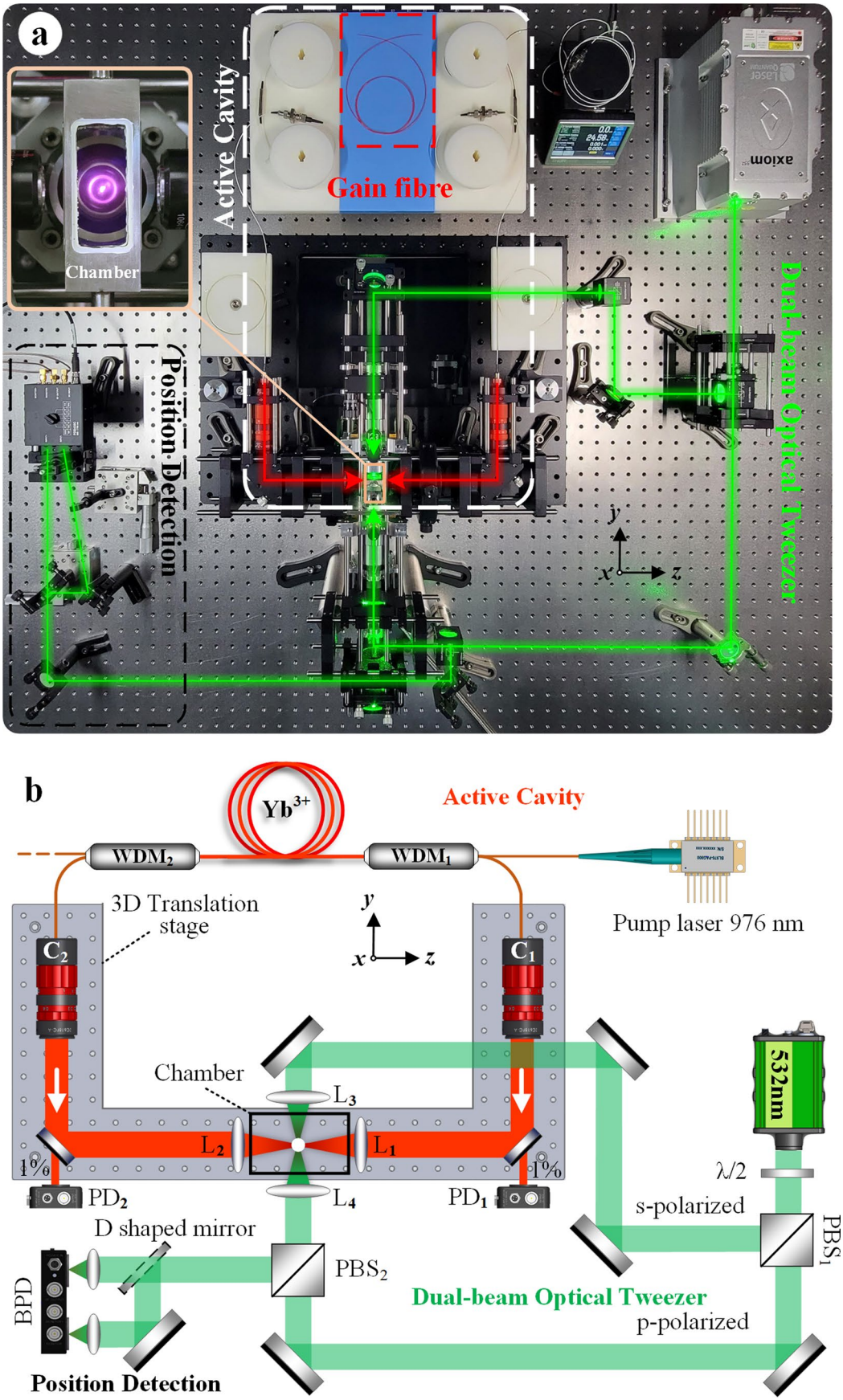

Extended Data Fig. 1 | Experimental setup. a, Photograph of the experimental setup on the *yoz* plane. Inset: the *xoz* plane of the chamber and lenses, where the bright spot reveals the intracavity laser (centre at 1030 nm) scattered by the trapped sphere. **b**, Schematic of the experimental system composed of a dual-beam optical tweezer (green) and an active cavity (red). WDM: wavelength division multiplexer, C: collimator, PBS: polarizing beam splitter, L_1-L_4: objectives, λ/2: half-wave plate, PD: Photodetector, BPD: balanced photodetector.